Article

Mapping the Speciation of Iron in *Pseudomonas aeruginosa* Biofilms Using Scanning Transmission X-ray Microscopy

Ryan C. Hunter, Adam P. Hitchcock, James J. Dynes, Martin Obst, and Terry J. Beveridge

Environ. Sci. Technol., **2008**, 42 (23), 8766-8772 • Publication Date (Web): 28 October 2008

Environ. Sci. Technol. **2008,** *42,* 8766–8772

Mapping the Speciation of Iron in *Pseudomonas aeruginosa* Biofilms Using Scanning Transmission X-ray Microscopy

RYAN C. HUNTER,*,‡,|| ADAM P. HITCHCOCK,§,|| JAMES J. DYNES,§,|| MARTIN OBST,§,|| AND TERRY J. BEVERIDGE†,‡,||

Molecular and Cellular Biology, University of Guelph, Guelph, Ontario, N1G 2W1, Brockhouse Institute for Materials Research, McMaster University, Hamilton, Ontario, L8S 4M1, and Advanced Food and Materials Network (AFMnet), Guelph, Ontario, N1G 2W1

Received June 17, 2008. Revised manuscript received September 11, 2008. Accepted September 22, 2008.

An important feature of microbial communities is the spatial heterogeneity of extracellular chemistry. Scanning transmission X-ray microscopy (STXM) was used to map the spatial distribution of iron species throughout *Pseudomonas aeruginosa* biofilms to assess the influence of chemical heterogeneity on biomineralization. *P. aeruginosa* biofilms were treated with Fe(III)-amended media. Speciation and quantitative mapping using STXM image sequences in the Fe $2p_{3/2}$ (L_3) absorption edge region revealed both Fe(II) and Fe(III) in localized microenvironments. Fe(III) was mainly associated with cell surfaces, while small amounts of Fe(II) was found in the extracellular space. Biofilms were also characterized using C 1s edge STXM image sequences. Anaerobic growth assays and confocal microscopy revealed the inability of *P. aeruginosa* to directly reduce Fe(III), implicating indirect iron reduction mechanisms in the formation of fine-grained, multivalent minerals. These studies suggest that geochemical microenvironments found throughout microbial communities are even more complex than previously believed.

Introduction

Bacteria are important mediators of geochemical processes for most elements in the periodic table (*1*). To date, most studies of these diverse processes have involved planktonic monocultures growing under conditions not normally encountered outside of the laboratory. This raises the question as to the applicability of such results to many environments because nutrient limitations and other stresses in natural environments frequently encourage bacteria to form biofilms. The physicochemical organization of these multicellular consortia is spatially and temporally complex and is quite different from the relatively homogeneous planktonic cultures studied in the laboratory (*2*). This complexity has prevented a comprehensive understanding of the fine-scale geochemistry of these communities.

A common approach to understanding these interactions is to determine bulk reaction conditions, such as pH and redox potential (Eh). This approach, while useful at a large scale, tells us little about mechanistic details at a fine spatial scale because cell physiology and reaction conditions are extremely heterogeneous (*3, 4*). Transmission electron microscopy (TEM) and energy dispersive X-ray spectroscopy (EDS) have been used to map elemental compositions of mineral deposits in bacterial communities at high resolution (*5, 6*); however, these techniques are unable to reveal oxidation states or the nature of ligands. Such information would help confirm small-scale extracellular chemistry (pH and Eh) conditions previously observed in *Pseudomonas aeruginosa* biofilms (*3, 7*).

Synchrotron-based X-ray spectromicroscopy is a promising technique that can both image and speciate microbially associated metals (*8, 9*). Scanning transmission X-ray microscopy (STXM), which employs near-edge X-ray absorption fine structure (NEXAFS) as its contrast mechanism, can be used to analyze hydrated biological samples with a spatial resolution of better than 30 nm (*10*). This is possible because of the ability of soft X-rays to penetrate water and suitable analytical core edges in the soft X-ray region. For the STXM microscopes used, spectral resolution is on the order of 100 meV at the C 1s edge. With suitable reference spectra, NEXAFS image sequences can be converted into quantitative maps of the chemical species present (*11*−*14*). Importantly, image sequences at metal 2p ($L_{2,3}$) edges can be used to map the valence states of metals in biological samples (*13*). This methodology is already being used for imaging chemically sensitive matter in a wide range of disciplines (*8*−*14*) and is an ideal technique for imaging bacteria and associated mineral phases in fully hydrated biofilms (*11, 13, 15*).

One limitation of STXM is that only relatively thin samples can be visualized, precluding the use of STXM on thick biofilm communities. We have previously attempted to circumvent this problem by embedding samples in a plastic resin and performing STXM on thin-sections to determine the speciation of iron throughout an entire biofilm (unpublished data). Unfortunately, embedding resins mask biological material spectral contrast, making it difficult to map using C 1s image sequences. Recently, it has been shown that TEM of frozen-hydrated sections also provides a means of visualizing prokaryotic structure at high-resolution (*16*). Though ultrastructure is best preserved if sections are viewed while frozen, carefully controlled freeze-drying of cryo-sections can also efficiently preserve ultrastructure (*17*). Here, we combine advantages of cryo-sectioning and freeze-drying with the analytical power of STXM to investigate the chemistry and partitioning of iron throughout *P. aeruginosa* biofilms.

We have previously utilized a number of approaches to localize microenvironments present throughout *P. aeruginosa* biofilms to help understand their geochemical influence (*3, 7, 18, 19*). Here, we work in the other direction, using STXM to map the distribution of the various minerals that form so as to establish the influence of chemical microenvironments on their development. This complementary information provides further insight into the contribution of microbial communities to geochemical cycling.

Materials and Methods

Bacterial Strains, Culture Conditions, and Biofilm Development. *P. aeruginosa* PAO1 was used throughout this study

* Corresponding author current address: Department of Biology, Massachusetts Institute of Technology, 77 Massachusetts Avenue, 68-380, Cambridge, MA 02139; phone: (617) 324-2773; fax: (617) 324-3972; e-mail: rchunter@mit.edu.
‡ University of Guelph.
§ McMaster University.
|| Advanced Food and Materials Network (AFMnet).
† Deceased.

10.1021/es801642z CCC: $40.75

Published on Web 10/28/2008

(J.S. Lam, University of Guelph). Growth was visualized using GFP (*3*). Dilute trypticase soy broth (dTSB) medium (3 g L^{-1}) was used for biofilm growth (unless indicated otherwise). Ultrapure deionized water (UDW, 18 MΩ cm^{-1}) was used to make all solutions. When possible, materials were leached of contaminating metals in 50% HNO_3 prior to use.

Biofilms were cultivated using two systems:

(a) Flow cells. A continuous culture flow cell was used as previously described (*3*). Biofilms were grown for 7 days with dTSB, dTSB containing 1% KNO_3, and dTSB containing 1 mM ferric citrate (pH 6.8). These biofilms were analyzed using confocal laser scanning microscopy.

(b) Silicone tubing. A dTSB solution (pH 6.8) was pumped through the silicone tubing (length = 1 m, diameter = 1 mm) via a peristaltic pump. Aluminum oxide discs (*19*) were implanted into the tubing and used for metal localization studies. Following a 24 h conditioning phase with dTSB, overnight cultures were inoculated by syringe. Cells were allowed to attach for 1 h before the flow of dTSB was initiated. After 7 days of growth, the medium was changed for 30 min to a 1 mM $Fe(NO_3)_3 \cdot 9H_20$ solution in dTSB (pH 6.8), followed by dTSB for 30 min. Effluent was collected, treatment and wash solutions combined, and were stored at −20 °C. Biomass was collected by squeezing the tubing along its entire length. These biofilms were analyzed using STXM and TEM.

For iron reduction experiments, cells were cultured anaerobically in dTSB, dTSB with 1% and 5% KNO_3, and dTSB supplemented with ferric citrate (1, 5, 10, and 20 mM). Tubes were shaken at 125 rpm at 25 °C.

Analytical Techniques and Growth Assays. A modified Ferrozine assay (*20*) was used to analyze iron speciation and total iron. Ferrozine (3-(-pyridyl)-5,6-diphenyl-1,2,4-triazine-*p,p*-disulfonic acid; 0.1 g L^{-1}) was prepared in 50 mM 4-(2-hydroxyethyl)-1-piperazineethanesulfonic acid (HEPES, pH 7.0). For Fe(II), a 1 mL sample was acidified with 1 mL of 0.5 N HCl for 1 h and centrifuged to remove cell debris before adding it to Ferrozine. For total Fe, 0.5 mL of sample was treated with 4.5 mL of 0.25 mM hydroxylamine in 0.25 mM HCl for 30 min. 0.1 mL of each fraction (Fe(II) and Fe_{TOT}) was added to 4.9 mL of Ferrozine. Color was developed for 30 min, and the absorbance was measured at 562 nm. Biofilm-associated metal was extracted with 0.5 M HCl as described previously (*6*).

Transmission Electron Microscopy (TEM) and Energy Dispersive X-ray Spectroscopy (EDS). Metal-treated biofilms were enrobed in 2% (wt/vol) Noble agar. Samples were fixed in 2% (vol/vol) glutaraldehyde for 1 h and were dehydrated through an ethanol series (25%, 50%, 75%, 95%, and 3 × 100%) for 15 min each. Samples were then treated with 50/50 ethanol/LR White for 30 min, and 100% LR White for another 30 min. Samples were then embedded in LR White-filled gelatin capsules for 1 h at 60 °C. Samples were sectioned and imaged as previously described (*19*). EDS was performed using an EDAX Sapphire retractable X-ray detector. EDS spectra were collected over 100 s (live count time) with a beam diameter of approximately 200 nm and a beam current of 25 mA.

STXM. Metal-treated biofilms collected from tubing were transferred into copper specimen tubes (Leica). Copper tubes were frozen using a Leica EM PACT high-pressure freezer and were stored under liquid nitrogen (<−135 °C). Frozen-hydrated sections were then processed as previously described (*16*). Cryo-sections were mounted in a Gatan cryoholder at −160 °C in a Philips EM400T TEM (100 kV). Temperature increases during lyophilization were controlled by a Gatan cold stage. Samples were gradually warmed up to 25 °C and imaged by TEM prior to STXM analysis.

Tubing biofilms were collected and shipped to the Canadian Light Source (CLS) (Saskatoon, Canada) for STXM analysis. A biofilm aliquot was placed onto an X-ray translucent silicon nitride membrane (1 × 1 mm pane, 75 nm thick; Norcada Inc.), covered with UDW, and a second membrane was placed on top. The silicon nitride sandwich was then sealed with a silicone sealant to form a wet cell.

X-ray spectromicroscopy was carried out using the interferometric-STXM/elliptically polarizing undulator beamline 10ID1 at the CLS (*21*). The freeze-dried sample was measured using the STXM microscope on bend magnet beamline 5.3.2 at the Advanced Light Source (Berkeley, CA) (*22*). STXM was used by recording images at selected single energies, image pairs (stack maps), or at a sequence of energies (image sequence, or stack mode) (*13, 14, 23*). Image sequences were converted to optical density using incident flux signals measured through regions of the wet cell that contained no biofilm. OD (x,y,E) data cubes were converted to quantitative component maps by spectral fitting using singular value decomposition (SVD) procedures (*24, 25*). These were recorded and put on absolute linear absorbance scales (*14*). The stack fit procedure (*10*) was used to fit the data to a sum of the spectra of expected constituent chemical species and an energy independent constant which accounts for possible differences in background levels of the reference and image sequence spectra. Reference compounds were those reported in earlier work (*11, 13*). Threshold masking of the derived Fe(II) and Fe(III) component maps was then used to extract spectra from pixels that had similar spectral characteristics, which were subjected to spectral curve fitting. The aXis2000 software package (http://unicorn.mcmaster.ca) was used for data and image processing.

Confocal Laser Scanning Microscopy. Biofilms were imaged as previously described (*3*).

Results and Discussion

Though several previous studies have used TEM/EDS to provide a high-resolution representation of the metal−microbe interactions that occur within a biofilm, the exact chemical identities of the precipitates that form have yet to be established. Here, we use STXM to elucidate chemical signatures of precipitates throughout *P. aeruginosa* biofilms to identify factors that may contribute to their formation. This technique has already been used to examine the distribution of biopolymers and metal species in natural communities (*11, 13*) and the nucleation of iron precipitates by microbial polysaccharides (*26*). Until now, however, this methodology has not been used to study a biofilm community whose physiology, extracellular polymers, and extracellular chemistry have been so extensively characterized (*3, 7, 18, 19*).

We have recently shown how heterogeneous sorption sites on cell surfaces can lead to a spatially complex organization of metal precipitates throughout a *P. aeruginosa* biofilm (*18*). Here we consider the possibility of the extracellular environmental conditions (i.e., pH and Eh) driving the formation of fine-grained minerals (possibly existing in different valence states). We use iron to investigate these interactions as it has a well-defined chemistry and readily precipitates throughout a biofilm. In solution, iron commonly exists as Fe(II) or Fe(III), and the relative amounts of these two valences are reflective of solution chemistry. For example, changes in pH have a significant impact on iron solubility, distribution, and reactivity. Specifically, within a biofilm, pH variation may alter chemical stability fields such that various mineral phases are thermodynamically driven to precipitate in localized microenvironments (*5, 6*). Changes in Eh can also partially determine the partitioning of metal ions between the solid and solution phase. As environments become anoxic, minerals such as iron hydroxides are particularly sensitive

to changes in redox and readily dissolve. In contrast, oxidizing conditions generally favor solid formation with associated sequestration of metals to growing mineral phases. pH and Eh changes initially affect microenvironments and the fine-grained minerals within them, but large microbial consortia might have much broader effects over time (e.g., contributing to large scale geological deposits) (*27*). Intuitively, determining the distribution and speciation of the fine-grained minerals that accumulate may be indicative of Eh and pH microenvironments that exist (or that once existed) throughout a biofilm community.

Bulk analysis was used to determine the amount of Fe(II) versus Fe(III) that accumulated in a biofilm after a 30 min treatment (see Table S1, Supporting Information). Silicone tubing alone did not adsorb Fe because there was no difference in the Fe concentration of the effluent compared to the treatment solution. When biofilms were treated with 1 mM $Fe(NO_3)_3$ solution, total iron in the effluent decreased by nearly 75% compared to the treatment solution (from 55 $\pm$ 4 μg/mL to 12 $\pm$ 5 μg/mL), which was subsequently observed to be retained by the biofilm. This demonstrated the efficiency of biofilm interfaces for metal sequestration. The $Fe(NO_3)_3$ treatment solution contained small amounts of Fe(II) (0.7 $\pm$ 0.3 μg/mL); however this amount did not change when passed through sterile tubing. This suggested that dTSB growth medium contained reducing components that resulted in a small amount of ferrous iron. In contrast, the metal-treated biofilm effluent was found to contain 6 $\pm$ 3 μg/mL Fe(II), indicating there was a transformation of Fe(III) to Fe(II) because of microbial activity. Somehow, Fe(III) was being reduced through processes mediated by the bacterial population.

TEM was used to localize the spatial distribution of iron precipitates throughout the biofilm using the natural electron density of Fe for contrast (Figure 1). Isolated clusters of cells accumulated small amorphous precipitates on their surfaces, as well as in the extracellular space. Interestingly, precipitates were present in a range of sizes and morphologies that appeared to be randomly distributed throughout the biofilm with no specific spatial organization. In addition, distinct microenvironments were observed in which few cells appeared to accumulate iron minerals on their surfaces, while the rest showed very little contrast from the surrounding medium (Figure 1b). These observations suggest that each cell in a biofilm is surrounded by a unique microenvironmental niche that results in a range of precipitates. Although EDS spectra revealed an iron signal from each precipitate (Figure 1a, inset), we were unable to identify the complexing counterion(s), nor could we identify the iron oxidation state. Other means were thus necessary to help correlate geochemical observations to microenvironmental conditions reported previously (*3, 7*).

We therefore used STXM to elucidate and map the chemical signatures of these precipitates in a wet cell preparation made of the PAO1 biofilm treated with $Fe(NO_3)_3$ (Figure 2). Figure 2a is the optical density image recorded at 288.2 eV, which reveals biological components dominated by the strong C 1s $\rightarrow \pi^*_{C=O}$ band of protein. This area was chosen for analysis based on large area survey difference maps (709.8−702 eV) (not shown), which rapidly identify areas of high Fe content. Figure 2b superimposes the difference image ($OD_{709} - OD_{704}$, blue) on the C 1s based map ($OD_{288.2} - OD_{282}$, green). It is evident that iron was abundant, with a strong Fe signal associated with only a few cells and the remainder of the Fe signal located in the extracellular space.

The spatial distribution of iron oxidation states was determined from an Fe 2p image sequence recorded in the region outlined in Figure 2b. The Fe(II) and Fe(III) distributions were derived by fitting the spectrum at each pixel to

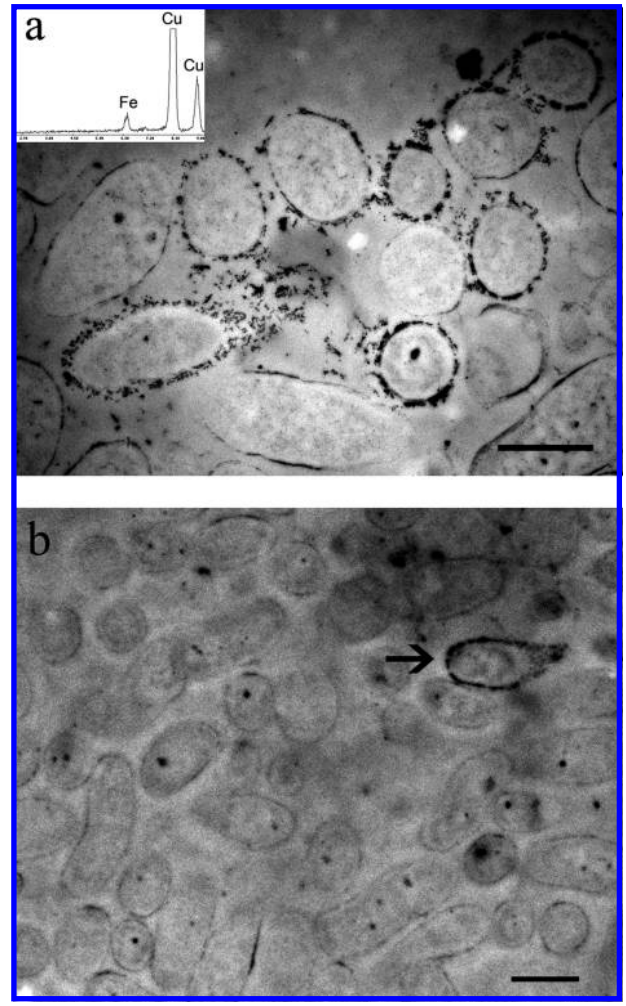

FIGURE 1. Transmission electron micrographs of thin sections through an iron-treated *P. aeruginosa* biofilm. Iron bound by the cells and mineralized in the extracellular space provides contrast. (a) Microcolony of cells showing a diversity of precipitates on their surfaces and in the extracellular space. (Inset) EDS spectrum obtained from the extracellular precipitates, showing peaks for iron. The large copper peaks were generated from the supporting TEM grid. (b) Lower magnification micrograph of a cell cluster in which few cells show fine-grained mineral formation on their surfaces (arrows). Heterogeneous metal accumulation/precipitation is indicative of discrete geochemical microenvironments in *Pseudomonas aeruginosa* biofilms. Bars = 1 μm.

the reference spectra (*13*). To confirm the validity of the analysis, Fe 2p spectra from Fe(II)-rich and Fe(III)-rich regions were extracted from the image sequence by threshold masking the Fe(II) and Fe(III) component maps (regions indicated by the color insert in Figure 2c). The adsorption signals of the extracted spectra were very weak, particularly in the Fe(II)-rich regions outside the cells, where the average Fe 2p peak intensity is only 1 milli-OD (0.001), while that in the region of strong Fe(III) signal was approximately 10 times larger (0.01 OD). Even so, by averaging over pixels with similar spectral signatures, well-defined spectra were generated (Figure 2c). Comparison of these spectra to reference compounds reveals that Fe(II) and Fe(III) spectral signatures exist, confirming the bulk speciation analysis.

Figure 3 presents results from a Fe 2p study of a different area of the same wet cell. Figure 3a is the sum of 18 images from 700−706 eV below the Fe 2p edge, where water and organics absorb. An Fe $2p_{3/2}$ image sequence was analyzed to generate Fe component maps, which are displayed in

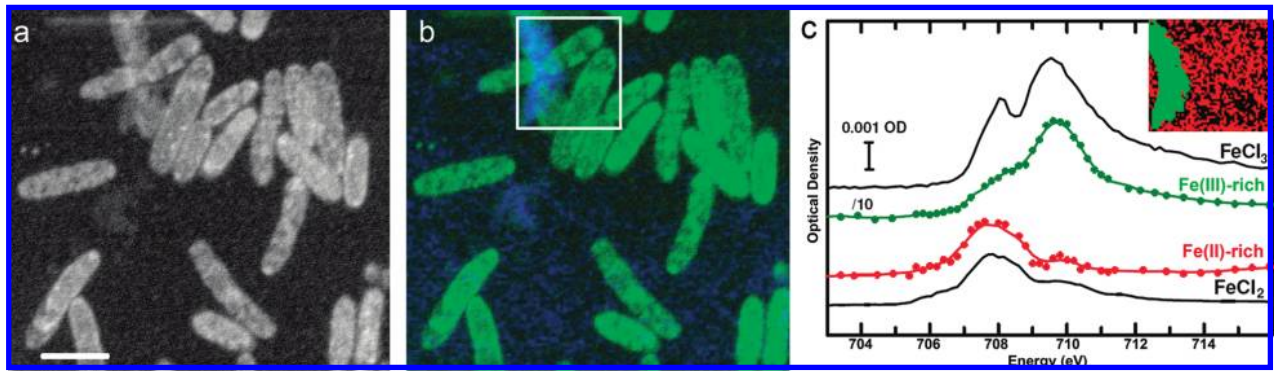

FIGURE 2. (a) Scanning transmission X-ray microscopy (STXM) image of a wet cell biofilm microcolony recorded at 288.2 eV (optical density representation). The horizontal trace in the upper left of the image is from radiation damage caused by a line scan spectrum used to probe the Fe oxidation states. Bar = 1 μm (b) STXM image of the same region at 709.8 eV (indicating OD associated with Fe(III)-rich regions) (in blue), superimposed on the OD image at 288.2 eV (in green). (c) Fe $2p_{3/2}$ X-ray absorption (NEXAFS) spectra from two reference compounds ($FeCl_2 \cdot 4H_2O$ and $FeCl_3 \cdot 6H_2O$) compared to spectra extracted from the regions indicated by the colored insert (green is Fe(III)-rich, red is Fe(II)-rich), indicating that both Fe(II) and Fe(III) are present within the biofilm. (CLS STXM).

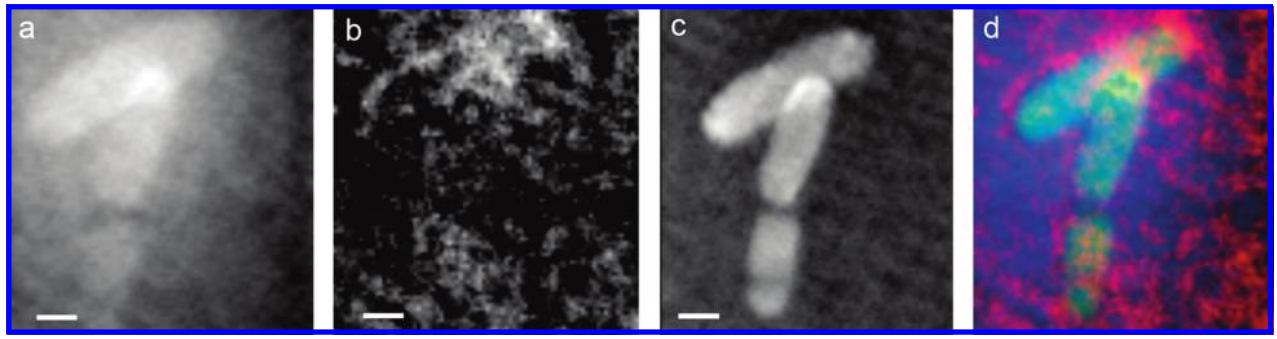

FIGURE 3. (a) Sum of 18 STXM images from 700−706 eV below the Fe 2p edge, where water and organics absorb. (b) Fe(II) and (c) Fe(III) component maps derived by fitting an Fe 2p image sequence (56 images from 700−718 eV, with 81 × 86 pixels − 50 nm pixel) to the reference spectra shown in Figure 2. These three images were combined to generate the color-coded spatial correlation composite map (d), with green indicating the organic phase (pre-Fe2p), red indicating the Fe(II) species, and blue indicating the Fe(III) species. Bars = 500 nm (CLS STXM).

Figure 3b and c. Fe(III) is predominantly associated with the bacterial cells while Fe(II) is present at a much lower level in the extracellular milieu adjacent to bacteria with strong Fe(III) levels. The segregation of iron species into specific regions of the biofilm is thus a common feature of *P. aeruginosa* communities.

Freeze-drying of vitreous sections has been shown to effectively preserve the structure of biological specimens when samples are warmed to room temperature (*17*). This method was used as an alternative to the wet cell observations that were performed on a disrupted biofilm. Prior to the STXM measurements, the freeze-dried metal-treated biofilms were imaged by TEM (Figure 4). Cells were visible, while electron density is also apparent in the extra-cellular space at higher magnification (inset, Figure 4). Sections were then examined by STXM, which generated quantitative biochemical and iron component maps based on measured C 1s and Fe 2p image sequences (Figure 5). First, the distributions of biological components were derived from the C 1s image sequence (Figure 5a). Macromolecular identity was confirmed by comparison to the C 1s signals of various reference compounds (Figure 5b). The C 1s signal from the bacteria is dominated by that of protein, while the polysaccharide and lipid components could only be convincingly identified after subtraction of the protein signal. This suggests some redistribution of the more delicate polysaccharide and lipid components may have occurred in the sample preparation procedure. However, we note that a previous study which employed correlative TEM and STXM imaging showed a total loss of organic material using conventional TEM preparation techniques (*11*). The cryo-preparation methods used here partially overcome this limitation.

The distribution of Fe oxidation states in the freeze-dried sample was determined from Fe 2p image sequences

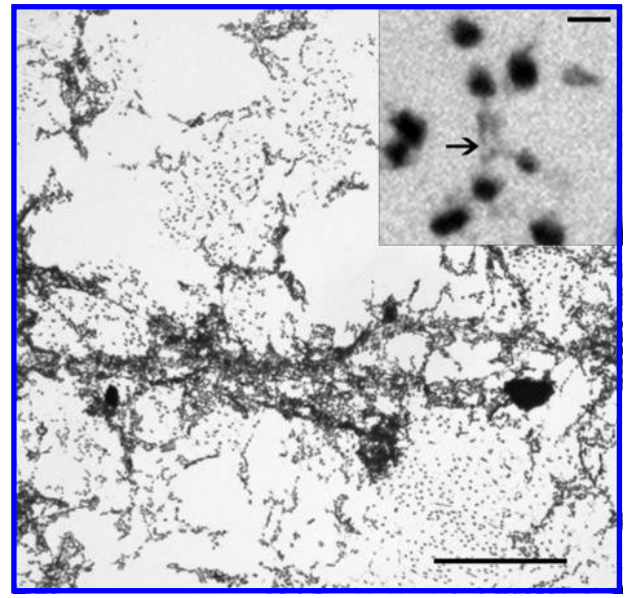

FIGURE 4. Transmission electron micrograph of a freeze-dried cryo-section of a *Pseudomonas aeruginosa* PAO1 biofilm treated with 1 mM $Fe(NO_3)_3$. Contrast is provided by iron bound to the cells/EPS. (Bar = 40 μm) At higher resolution (inset), iron can be seen to precipitate both in association with the cells and in the extracellular space (arrow) (Bar = 1 μm). This freeze-dried section was subsequently analyzed by STXM.

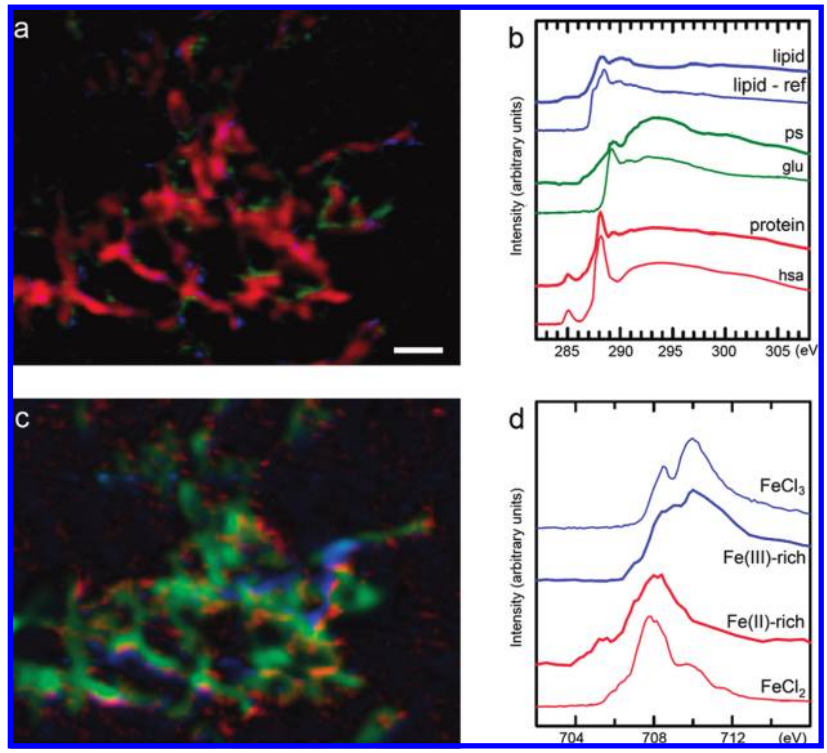

FIGURE 5. (a) Color-coded composite map of a freeze-dried *P. aeruginosa* biofilm cryosection derived from a STXM C 1s image sequence (96 images from 280−320 eV; 60 nm pixels, 1 ms/pixel). Red = protein; green = polysaccharide (ps); blue = lipid. Bar = 1 μm. (b) C 1s spectra extracted from the image sequence, compared to the reference standards used to generate the component maps. Note that the biofilm-derived spectra for polysaccharide-rich (80%) and lipid-rich (90%) regions displayed have had a large protein signal (>80% of the as-extracted signal) subtracted. (c) Composite map of Fe(II), Fe(III), and non-Fe components derived from an Fe 2p image sequence recorded in the same region as Figure 5a. (red = Fe(II), green = non-Fe, blue = Fe(III)). (d) Fe $2p_{3/2}$ spectra extracted from the image sequence, compared to reference standards (48 images from 700−717 eV; 60 nm pixels, 3 ms/pixel)). (ALS STXM5.3.2).

recorded from the same cell cluster. Derived component maps (Figure 5c and d) once again revealed the presence of both Fe valences. In this case, it should be noted that electron beam dosage may have caused the partial reduction of Fe(III); however, the presence of both oxidation states is consistent with bulk chemistry and wet cell observations, which were not exposed to the TEM beam. The presence of Fe(III) was expected because we had previously measured highly oxidizing conditions and circumneutral pH throughout *P. aeruginosa* biofilms (*3, 7*). However, these conditions would theoretically shift the equilibrium toward Fe(III) and prevent the reduction of iron to Fe(II). The fact that ferrous iron is present in most areas examined suggests one of the following: (a) iron was being directly reduced by the bacteria or (b) chemical microenvironments exist (below the resolution limits of the chemically sensitive probes) that drive the reduction of Fe(III). The latter would indicate chemical heterogeneity exists that is far beyond the detection limits of conventionally used approaches.

Two approaches were used to determine if the presence of Fe(II) was the result of direct enzymatic reduction by the bacteria themselves. First, PAO1 was grown under anaerobic conditions in dTSB, dTSB supplemented with 1% and 5% KNO_3, and dTSB supplemented with ferric citrate. Growth curves revealed that anaerobic growth does not occur with dTSB alone or with supplementation of the growth medium with Fe(III) citrate (data not shown). As expected, reduction of NO_3^- as an electron acceptor was the only growth condition that showed an increase in cell density, implying that *P. aeruginosa* PA01 cannot utilize direct Fe(III)-reduction for growth. To confirm these results, Gfp-tagged *P. aeruginosa* biofilms were grown in a flow cell with dTSB alone, dTSB with 1% KNO_3, and dTSB supplemented with 1 mM ferric citrate (Figure 6). These biofilms were then analyzed by CSLM. Because the addition of KNO_3 resulted in a biofilm thickness over twice that of

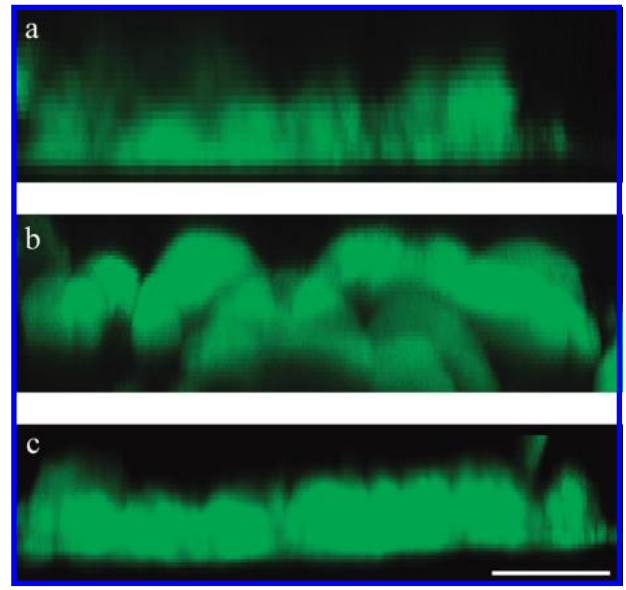

FIGURE 6. CLSM images of GFP-labeled *P. aeruginosa* PAO1 biofilms grown in (a) dTSB, (b) dTSB supplemented with 0.5% KNO_3, and (c) dTSB supplemented with 1 mM ferric citrate. No difference in biofilm morphology is apparent between unsupplemented growth conditions and dTSB supplement with 1 mM ferric citrate, suggesting that iron reduction does not support anaerobic growth in *P. aeruginosa* communities. Bar = 40 μm.

a biofilm grown in dTSB (Figure 6b), it is possible that the addition of NO_3^- is supporting growth in oxygen-restricted regions of the biofilm. If PAO1 was able to utilize Fe(III) as an electron acceptor, a similar result would be expected. As shown in Figure 6c, this was not the case. Biofilms grown in dTSB and dTSB supplemented with 1 mM ferric citrate showed no obvious differences in community structure or thickness. Transport and energy yield of each oxidant is expected to be different, which may also be contributing to community structure, but together these observations provide no evidence to suggest that the Fe(II) present in the extracellular regions of the *P. aeruginosa* biofilms was a result of reduction via anaerobic respiration. It is possible, however, that Fe(III) was reduced through extracellular electron transfer mechanisms (*28*). Indeed, when the planktonic growth medium was concurrently analyzed using the FerroZine assay, small amounts of Fe(II) were detectable over the 60 h growth period (approximately 8% of Fe_{TOT}). These amounts are significantly less than those found via bulk analysis of the biofilms, but it is conceivable that shuttling or extracellular electron transfer mediated by the bacteria is at least partially responsible for the production of multivalent fine-grained mineral phases.

The results presented here are best explained by the presence of localized geochemical microenvironments that result in a spatially heterogeneous distribution of metal precipitates throughout a microbial community. In general, the presence of both Fe(II) and Fe(III) species is indicative of microbes using Fe(III) as an energy source via electron transfer mechanisms. However here we show experimental evidence that this is not always the case. Rather, biofilm microbes may generate the observed multiple iron valence states through conditioning their localized extracellular microenvironments to a degree where nonenzymatic iron reduction is possible. Since pH and Eh are known to have a profound influence on solution chemistry, the heterogeneity of chemical conditions found throughout microbial biofilms may be as important as direct oxidation/reduction in the mediation of metal speciation throughout the bulk environments. By locally mediating solution chemistry, subpopulations of microbes within a biofilm may ultimately determine the state and availability of a metal. This could help explain why different mineral phases that form only under discrete geochemical conditions (e.g., goethite, hematite) can be found within micrometers of one another (*5*). The pH/Eh distribution that we have found in previous studies, however, is not sufficient to explain the mineral distributions shown here. Instead, these experiments suggest that even smaller-scale microenvironments (approaching a "nano"-environment scale) could exist throughout biofilm communities that are undetectable by conventional methods. In this sense, the identification of metal speciation may be a more reliable indicator of the microenvironmental history than the use of present-day chemical or physical probes.

The use of STXM as a probe of the fine-scale geochemistry is particularly powerful because it allows submicron measurements to be performed on fully hydrated biofilms. Clearly, the continued development of this technique will help elucidate further linkages between biofilm and geochemical processes on a range of spatial and temporal scales. Here, we use the technique to help explain previous small-scale laboratory experiments that have proposed the microenvironment−geochemistry relationship (*5, 6*). In each case, various mineral phases possessing remarkably different stability fields were found within microns of one another and exemplify the fine control that microbes have over their extracellular environment. Each study suggests that various microbiologically aided chemical and redox conditions helped lead to some present-day large-scale mineral formations, but there is little direct evidence to support these claims. The question remains open but it is essential to fully understand biofilm−metal interactions at as fine a degree as possible because they might serve as small-scale analogues (*27*). Certainly, over geological time, it is plausible that the microenvironmental effect is enormous and may have been an important factor in the formation of large scale mineral deposits.

Acknowledgments

This work was funded through NSERC—Discovery, NSERC-Major Facilities Access, US-DOE and Advanced Food and Materials Network grants. The STXM microscope is supported by NSF, DMR-9975694, DOE DE-FG02-98ER45737, Dow Chemical, NSERC, and the CFI. We thank Chithra Karunakaran, Kon Kaznatcheev, and Drew Bertwistle for maintaining the CLS STXM and David Kilcoyne and Tolek Tyliszczak for their contributions to the ALS STXMs. The ALS is supported by the Director, Office of Energy Research, Office of Basic Energy Sciences, Materials Sciences Division of the US-DOE, under Contract No. DE-AC03-76SF00098. The CLS is supported by NSERC, CIHR, NRC, and the University of Saskatchewan.

Supporting Information Available

Bulk Ferrozine analysis of iron concentrations and speciation in metal treatment solutions and biofilm biomass. This material is available free of charge via the Internet at http://pubs.acs.org.

Literature Cited

(1) Silver, S. The bacterial view of the periodic table: specific functions for all elements In *Geomicrobiology: Interactions between Microbes and Minerals*; Banfield, J. F., Nealson, K. H., Eds.; Mineralogical Society of America: Washington, DC, 1997; pp 345−360.

(2) Davey, M. E.; O'Toole, G. A. Microbial biofilms: From ecology to molecular genetics. *Microbiol. Mol. Biol. Rev.* **2000**, *64*, 847–867.

(3) Hunter, R. C.; Beveridge, T. J. Application of a pH-sensitive fluoroprobe (C-SNARF-4) for pH microenvironment analysis in *Pseudomonas aeruginosa* biofilms. *Appl. Environ. Microbiol.* **2005**, *71*, 2501–2510.

(4) Xu, K. D.; Stewart, P. S.; Xia, F.; Huang, C. T.; McFeters, G. A. Spatial physiological heterogeneity in *Pseudomonas aeruginosa* biofilm is determined by oxygen availability. *Appl. Environ. Microbiol.* **1998**, *64*, 4035–4039.

(5) Brown, D. A.; Kamineni, D. C.; Sawicki, J. A.; Beveridge, T. J. Minerals associated with biofilms occurring on exposed rock in a granitic underground research laboratory. *Appl. Environ. Microbiol.* **1994**, *60*, 3182–3191.

(6) Lee, J.-U.; Beveridge, T. J. Interaction between iron and *Pseudomonas aeruginosa* biofilms attached to Sepharose surfaces. *Chem. Geol.* **2001**, *180*, 67–80.

(7) Hunter, R. C. The influence of *Pseudomonas aeruginosa* biofilm microenvironments on metal-microbe interactions. Ph.D. Thesis, University of Guelph, Guelph, Ontario, Canada, 2007.

(8) Glasauer, S.; Langley, S.; Boyanov, M.; Lai, B.; Kemner, K.; Beveridge, T. J. Mixed valence cytoplasmic iron granules linked to anaerobic respiration. *Appl. Environ. Microbiol.* **2007**, *73*, 993–996.

(9) Geesey, G. G.; Borch, T.; Reardon, C. L. Resolving biogeochemical phenomena at high spatial resolution through electron microscopy. *Geobiology* **2008**, *6*, 263–269.

(10) Hitchcock, A. P.; Moran, C.; Zhang, X.; Araki, T.; Dynes, J.; Stover, H.; Brash, J.; Lawrence, J. R.; Leppard, G. G. Soft X-ray spectromicroscopy of biological and synthetic polymer systems. *J. Elec. Spectrosc. Rel. Phenom.* **2005**, *144* 259–269.

(11) Lawrence, J. R.; Swerhone, G. D. W.; Leppard, G. G.; Araki, T.; Zhang, X.; West, M. M.; Hitchcock, A. P. Scanning transmission X-ray, laser scanning, and transmission electron microscopy mapping of the exopolymeric matrix of microbial biofilms. *Appl. Environ. Microbiol.* **2003**, *69*, 5543–5554.

(12) Ade, H. X-ray spectromicroscopy In *Experimental Methods in the Physical Sciences*; Samson, J., Ederer, D., Eds.; Academic Press: San Diego, 1998; Vol. 32.
(13) Dynes, J. J.; Tyliszczak, T.; Araki, T.; Lawrence, J. R.; Swerhone, G. D. W.; Leppard, G. G.; Hitchcock, A. P. Speciation and quantitative mapping of metal species in microbial biofilms using scanning transmission X-ray microscopy. *Environ. Sci. Technol.* **2006**, *40*, 1556–1565.
(14) Ade, H.; Hitchcock, A. P. NEXAFS microscopy and resonant scattering: Composition and orientation probed in real and reciprocal space. *Polymer* **2008**, *49*, 643–675.
(15) Toner, B.; Fakra, S.; Villalobos, M.; Warwick, T.; Sposito, G. Spatially resolved characterization of biogenic manganese oxide production within a bacterial biofilm. *Appl. Environ. Microbiol.* **2005**, *71*, 1300–1310.
(16) Matias, V. R. F.; Al-Amoudi, A.; Dubochet, J.; Beveridge, T. J. Cryo-transmission electron microscopy of frozen-hydrated sections of *Escherichia coli* and *Pseudomonas aeruginosa*. *J. Bacteriol.* **2003**, *185*, 6112–6118.
(17) Schultz, M.; Rudolf, F.; Gallitelli, M. F. Improvement in quantitative X-ray microanalysis of biological cryosections. *Microsc. Microanal.* **1999**, *5*, 187–196.
(18) Hunter, R. C.; Phoenix, V. R.; Beveridge, T. J. Impact of growth environment and physiological state on metal immobilization by *Pseudomonas aeruginosa* PAO1 *Microbiology* **2008**, Submitted.
(19) Hunter, R. C.; Beveridge, T. J. High-resolution visualization of *Pseudomonas aeruginosa* PAO1 biofilms by freeze-substitution transmission electron microscopy. *J. Bacteriol.* **2005**, *187*, 7619–7630.
(20) Lovley, D. R.; Phillips, E. J. P. Rapid assay for microbially reducible ferric iron in aquatic sediments. *Appl. Environ. Microbiol.* **1987**, *53*, 1536–1540.
(21) Kaznatcheev, K. V.; Karunakaran, Ch.; Lanke, U. D.; Urquhart, S. G.; Obst, M.; Hitchcock, A. P. Soft X-ray spectromicroscopy beamline at the CLS: Commissioning results. *Nucl. Inst. Meth. A* **2007**, *582*, 96.
(22) Kilcoyne, A. L. D.; Tyliszczak, T.; Fakra, S.; Hitchcock, P.; Franck, K.; Anderson, E.; Harteneck, B.; Rightor, E. G.; Mitchell, G. E.; Hitchcock, A. P.; Yang, L.; Warwick, T.; Ade, H. Interferometrically controlled scanning transmission microscopes at the advanced light source. *J. Synchroton Radiat.* **2003**, *10*, 125–136.
(23) Jacobsen, C.; Wirick, S.; Flynn, G.; Zimba, C. Soft X-ray spectroscopy from image sequences with sub-100 nm spatial resolution. *J. Microsc.* **2000**, *197*, 173–184.
(24) Press, W. H.; Flannery, B. P.; Teukolsky, S. A.; Vetterling, W. T. *Numerical Recipes in C: The Art of Scientific Computing*; Cambridge University Press: Cambridge, U.K., 1992.
(25) Strang, G. *Linear Algebra and Its Applications*; Harcourt Brace Jovnovich: San Diego, CA, 1988.
(26) Chan, C. S.; De Stasio, G.; Welch, S. A.; Girasole, M.; Frazer, B. H.; Nesterova, M. V.; Fakra, S.; Banfield, J. F. Microbial polysaccharides template assembly of nanocrystal fibers. *Science.* **2004**, *303*, 1656–1658.
(27) Konhauser, K. O.; Hamade, T.; Raiswell, R.; Morris, R.; Ferris, F. G.; Southam, G.; Canfield, D. E. Could bacteria have formed the Precambrian banded iron formations? *Geology* **2002**, *30*, 1079–1082.
(28) Wang, Y.; Newman, D. K. Redox reactions of phenazine antibiotics with ferric (hydr)oxides and molecular oxygen. *Environ. Sci. Technol.* **2008**, *42*, 2380–2386.

ES801642Z